

Electrodynamic calculations of spontaneous emission coupled to metal nanostructures of arbitrary shape: nanoantenna-enhanced fluorescence

Vincenzo Giannini,¹ José A. Sánchez-Gil,^{1,*} Otto L. Muskens,² and Jaime Gómez Rivas²

¹*Instituto de Estructura de la Materia, Consejo Superior de Investigaciones Científicas, Serrano 121, 28006 Madrid, Spain*

²*Foundation for Fundamental Research on Matter (FOM) Institute for Atomic and Molecular Physics (AMOLF), c/o Philips Research Laboratories, High Tech Campus 4, 5656 AE, Eindhoven, The Netherlands*

*Corresponding author: j.sanchez@iem.cfmac.csic.es

Received January 8, 2009; revised May 22, 2009; accepted May 23, 2009; published July 15, 2009

We present a theoretical study of the spontaneous emission of an optical emitter close to a metal nanostructure of arbitrary shape. The modification of the corresponding radiative and nonradiative decay rates and resulting quantum efficiencies, expressed on the basis of a semiclassical dipole model in terms of the local plasmonic mode density, is calculated by means of the rigorous formulation of the Green's theorem surface integral equations. Metal losses and the intrinsic nonradiative decay rate of the molecules are properly considered, presenting relationships valid in general for arbitrary intrinsic quantum yields. Resonant enhancement of the radiative and nonradiative decay rates of a fluorescent molecule is observed when coupled to an optical dimer nanoantenna. Upon varying the dipole position, it is possible to obtain a predominant enhancement of radiative decay rates over the nonradiative counterpart, resulting in an increase of the internal quantum efficiency. For emitters positioned in the gap, quantum efficiency enhancements from an intrinsic value of 1% to ~75% are possible. © 2009 Optical Society of America

OCIS codes: 240.6680, 160.4236, 260.2510, 290.5850.

1. INTRODUCTION

The properties of spontaneous emission of an excited atom depend not only on the wave function of the quantum system but also on the surrounding media. The spontaneous emission rate of an optical emitter is connected to the local photonic mode density, as given by Fermi's golden rule [1]. Systems that modify the density of modes are currently of great interest. The simplest system one may think of is a flat reflecting substrate, which has been extensively studied since long ago in the context of surface-enhanced fluorescence and energy transfer [2–5]; later on, increasingly complex systems such as metal films and structured dielectric/metallic surfaces were also thoroughly investigated [5–8]. In most cases, however, quenching associated with the enhancement of nonradiative decay rates plays a limiting role [3].

In recent years, metallic nanostructures have been theoretically proposed as candidates to strongly drive spontaneous emission [9–13]; various experimental works have indeed confirmed enhanced fluorescence close to metal nanoparticles [14–16], allowing in turn for single molecule spectroscopy. The excitation of localized surface plasmons (collective modes of the metal electron plasma) in metal nanostructures [17–19] are responsible for the strong modification of the local density of electromagnetic states. In this regard, the concept of optical nanoantennas has been indeed coined, analogous to radio wave antennas, to stress the ability of metal nanoparticles to convert visible light into localized electromagnetic energy and

vice versa [20–28]. It is crucial in plasmon-enhanced fluorescence to achieve efficient radiative outcoupling of localized surface plasmons into photons rather than the mere coupling of the emitter to plasmon modes. The advantage of optical dimer nanoantennas with strong geometric resonances stems both from high radiative efficiency while keeping nonradiative absorption weaker and large local field enhancements in the narrow gap between the two coupled nanoparticles [16]. Recall that an efficient design of metal nanoantennas to significantly enhance the quantum yield of low-efficiency emitters has straightforward implications in, e.g., (bio)molecular sensing or optoelectronic devices.

In this work we investigate the spontaneous emission rate of a single optical emitter in the vicinity of arbitrary shaped nanostructures. On the one hand, we make use of a scattering formulation that allows us to deal with an arbitrary number of scatterers of complex shapes. On the other hand, we take into account that the intrinsic quantum efficiency can take any value $\leq 100\%$ and express the radiative and nonradiative decay rates and quantum efficiency in terms of the local density of electromagnetic states and total scattered power. In this manner we can calculate all relevant magnitudes for a variety of optical emitters (fluorescence molecules, quantum dots, etc.) close to nanoantennas.

This work is organized as follows. In Section 2 we present the derivation of the expression of the decay rate from the local density of electromagnetic states obtained

from the electric field generated by a point dipole coupled to the metal nanostructure back at its position; this is calculated by means of the Green's theorem surface integral equation formulation in parametric form. We also present a useful set of formulae to determine separately the radiative and nonradiative decay rates, properly normalized, for an optical emitter with arbitrary intrinsic efficiency. In Section 3 we exploit the above formulation to carry out calculations of single molecule fluorescence enhanced by a metallic dimer nanoantenna in different configurations, revealing the most favorable ones to achieve large enhancements of radiative decay rates and/or quantum efficiencies. Finally, the conclusions are drawn in Section 4.

2. THEORETICAL MODEL

In this section, we show how to obtain the emission properties of an optical emitter near a metal nanostructure of complex shape. This can be studied by considering the interaction of a classical oscillating dipole with the electromagnetic field scattered by the nanostructure. This approach has been successfully used in various works [2,3,5–7,9,11,16,29]; despite being a classical model, it yields decay rates in full agreement with the quantum description [4,7]. The electromagnetic field generated by a dipole source and scattered by the nanostructures is calculated by means of the rigorous formulation of the Green's theorem surface integral equations in parametric form [30].

A. Spontaneous Decay Rate

The equation of motion of a dipole source is described as a harmonically bound charge with dipole moment \mathbf{p} forced by a local field \mathbf{E}_{loc} ,

$$\frac{d^2\mathbf{p}}{dt^2} + \omega^2\mathbf{p} + \gamma_0\frac{d\mathbf{p}}{dt} = \frac{e^2}{m}[\mathbf{p}_0^* \cdot \mathbf{E}_{\text{loc}}]\frac{\mathbf{p}_0}{p_0^2}, \quad (1)$$

where ω is the oscillation frequency in the absence of damping, γ_0 is the damping rate (inverse lifetime τ_0^{-1}) for the free dipole, m is the dipole effective mass, and e is the electron charge.

In the absence of a nanostructure, the right-hand side of Eq. (1) is null, thus retrieving the free dipole expression, which can be written in this form:

$$\mathbf{p}(t) = \mathbf{p}_0 e^{-i\omega t} e^{-(\gamma_0/2)t}. \quad (2)$$

The decay rate γ_0 has two contributions,

$$\frac{1}{\tau_0} = \gamma_0 = \gamma_{r0} + \gamma_{nr0}, \quad (3)$$

where γ_{r0} is the intrinsic radiative decay rate, accounting for electromagnetic power radiated in the far-field. γ_{nr0} is the intrinsic nonradiative decay rate, accounting for internal energy dissipation. It is possible to obtain the free radiative decay rate by means of the classical electrodynamic approach [31]

$$\gamma_{r0} = \frac{2ne^2}{3mc^3}\omega^2, \quad (4)$$

where $n = \sqrt{\epsilon}$ is the refractive index of the medium containing the dipole. The intrinsic quantum efficiency η_0 is thus defined as

$$\eta_0 = \frac{\gamma_{r0}}{\gamma_0}. \quad (5)$$

Equation (5) represents the spontaneous emission probability.

In the presence of the nanostructure, the right-hand side of Eq. (1) is different from zero, and the resulting dipole moment can be written as

$$\mathbf{p}(t) = \mathbf{p}_0 e^{-i\Omega t} = \mathbf{p}_0 e^{-i\omega' t} e^{-(\gamma/2)t}, \quad (6)$$

where Ω is the complex oscillation frequency of the dipole when the nanostructure is present, its imaginary part γ being the modified decay rate. The dipole moment \mathbf{p} and the local electric field \mathbf{E}_{loc} oscillate at the same frequency, so that

$$\mathbf{E}_{\text{loc}}(t) = \mathbf{E}_0 e^{-i\Omega t}. \quad (7)$$

Upon substituting Eqs. (6) and (7) into Eq. (1), the complex frequency Ω is obtained:

$$\Omega = -i\frac{\gamma_0}{2} + \omega \sqrt{1 - \frac{\gamma_0^2}{4\omega^2} - \frac{e^2}{p_0^2 m \omega^2} \mathbf{p}_0^* \cdot \mathbf{E}_0}. \quad (8)$$

As expected, when ($\mathbf{E}_0=0$) and there is no damping, we recover the free dipole oscillation frequency $\Omega=\omega$. Now we note [32] that γ_0^2 and $e^2/(p_0^2 m)$ are both very small compared to ω^2 , so an expansion of the square root is appropriate, yielding the following results:

$$\Delta\omega \equiv \omega - \omega' = \frac{\gamma_0^2}{8\omega} + \frac{e^2}{2p_0^2 m \omega} \Re(\mathbf{p}_0^* \cdot \mathbf{E}_0), \quad (9a)$$

$$\gamma = \gamma_0 + \frac{e^2}{m\omega p_0^2} \Im(\mathbf{p}_0^* \cdot \mathbf{E}_0). \quad (9b)$$

Equation (9a) determines the frequency shift of the dipole emission when the nanostructure is present; this frequency shift is nearly negligible for most cases of physical relevance, assuming that $\omega'=\omega$ is a good approximation. In addition, a full quantum mechanical expression for $\Delta\omega$ that differs from Eq. (9a) is necessary in general [7]. Equation (9b) represents the decay rate variation of the free dipole coupled to the nanoantenna. We are interested in the decay rate enhancements, so it is convenient to normalize it by the decay rate emission of a free dipole; by using Eq. (5) we obtain

$$\frac{\gamma}{\gamma_0} = 1 + \frac{3\eta_0 c^3}{2p_0^2 n \omega^3} \Im(\mathbf{p}_0^* \cdot \mathbf{E}_0). \quad (10)$$

We can see that only the reflected electromagnetic field at the dipole position is necessary to calculate the spontaneous emission variations. Essentially, the imaginary part of the local field yields the local electromagnetic density of

states, in agreement with the expression for γ obtained from quantum mechanical formulations [4,7].

Similarly to the free dipole, the decay rate γ is constituted by radiative and nonradiative components. In the nonradiative decay rate, the losses due to the nanostructure absorption must be considered. We can thus write the decay rate γ in this manner:

$$\gamma = \frac{1}{\tau} = \gamma_{nr0} + \gamma_{nr} + \gamma_r, \quad (11)$$

where γ_r is the radiative decay rate when the nanoantenna is present, and γ_{nr} is the nonradiative decay rate due to the nanoantenna absorption. Therefore, the quantum efficiency or apparent quantum yield, i.e., the probability that a photon be spontaneously emitted, is:

$$\eta = \frac{\gamma_r}{\gamma_{nr0} + \gamma_{nr} + \gamma_r}; \quad (12)$$

which, if normalized by that of a free dipole, the intrinsic quantum efficiency in Eq. (5) can be expressed as

$$\frac{\eta}{\eta_0} = \frac{\gamma_r/(\gamma_{nr} + \gamma_r + \gamma_{nr0})}{\gamma_{r0}/(\gamma_{r0} + \gamma_{nr0})} = \frac{\gamma_0}{\gamma} \frac{\gamma_r}{\gamma_{r0}}. \quad (13)$$

B. Electromagnetic Field Scattered by a Dipole

It has been shown that the decay rate variations are obtained from the imaginary part of the reflected electromagnetic field at the dipole position, i.e., the local density of electromagnetic states. To this end, we calculate the electromagnetic field scattered from a nanostructure illuminated by a nearby dipole source (see Fig. 1) by means of the rigorous formulation of the Green's theorem surface integral equations. Actually, with this method it is possible to solve the scattering problem for a complex shape of the nanostructure, as will be shown in the next subsection. Once the scattering problem is solved, the decay rates γ_r and γ_{nr} can be obtained.

In the following, we restrict ourselves to bidimensional geometries for the sake of computational effort. We consider the case of a p -polarized dipole source, since this polarization permits to excite plasmon resonances (see Fig. 1). In such a case, the magnetic field presents only one nonzero component (y component); the Helmholtz wave equation for the magnetic field has the form

$$\nabla^2 \mathbf{H} + k^2 \mathbf{H} = -\frac{4\pi}{c} \nabla \times \mathbf{J}. \quad (14)$$

\mathbf{J} is the charge current density of a free dipole [31]:

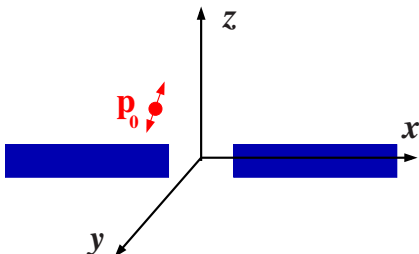


Fig. 1. (Color online) Illustration of the scattering geometry for a dipole source \mathbf{p}_0 in the vicinity of a dimer nanoantenna.

$$\nabla \cdot \mathbf{J} = -\frac{\partial \rho}{\partial t}, \quad (15a)$$

$$\rho(\mathbf{r}, \omega) = -\mathbf{p}_0 \cdot \nabla \delta(\mathbf{r} - \mathbf{r}_0) e^{-i\omega t}, \quad (15b)$$

where \mathbf{r}_0 and ρ are the position and charge of the dipole.

Employing Green's integral theorem inside and outside the metal, and proceeding as in [30], we obtain the system of coupled integral equations:

$$H^{(\text{dip})}(\mathbf{R}_l, \mathbf{r}_0) + \frac{1}{4\pi} \sum_j \int_{\Gamma_j} \left[\mathcal{H}_j(t) \frac{\partial G^{(\text{out})}(\mathbf{R}_l, \mathbf{R}_j(t))}{\partial N_j} - G^{(\text{out})}(\mathbf{R}_l, \mathbf{R}_j(t)) \mathcal{L}_j(t) \right] dt = \mathcal{H}_l(t), \quad l = 1, \dots, N, \quad (16a)$$

$$\frac{1}{4\pi} \int_{\Gamma_j} \left[\mathcal{H}_j(t) \frac{\partial G_j^{(\text{in})}(\mathbf{R}_l, \mathbf{R}_j(t))}{\partial N_j} - \frac{\varepsilon_j^{(\text{in})}(\omega)}{\varepsilon(\omega)} \times G_j^{(\text{in})}(\mathbf{R}_l, \mathbf{R}_j(t)) \mathcal{L}_j(t) \right] dt = 0, \quad l, j = 1, \dots, N. \quad (16b)$$

In the latter equations, $H^{(\text{dip})}$ is the incident field of the dipole and \mathcal{H}_j and \mathcal{L}_j are the (unknown) source functions, to be defined below. The other variables and functions correspond to the following: Γ_j is the surface profile of the j -th scatterer, given as parametric curves by the continuous vector-valued function $\mathbf{R}_j(t) \equiv (\xi_j(t), \eta_j(t))$, where (ξ_j, η_j) are the coordinates of a point of the profile in the xz plane; $\partial/\partial N_j$ is the normal derivative; and the Green's functions in the surrounding media $G^{(\text{out})}$ and within each one of the j -th scatterers $G_j^{(\text{in})}$ with refractive index $n_j = \sqrt{\varepsilon_j^{(\text{in})}}$ are given by the zeroth-order Hankel function of the first kind as follows:

$$G^{(\text{out})}(\mathbf{r}, \mathbf{R}) = i\pi H_0^{(1)} \left[\frac{\omega}{c} \sqrt{\varepsilon} |\mathbf{r} - \mathbf{R}| \right], \quad (17a)$$

$$G_j^{(\text{in})}(\mathbf{r}, \mathbf{R}) = i\pi H_0^{(1)} \left[\frac{\omega}{c} \sqrt{\varepsilon_j^{(\text{in})}} |\mathbf{r} - \mathbf{R}| \right]. \quad (17b)$$

Incidentally, it should be recalled that the presence of a flat substrate can be accounted for within this formulation by introducing the corresponding Green's function $G^{(\text{out})}$.

The unknowns of the coupled integral equations in Eqs. (16) are the surface field functions \mathcal{H}_j and \mathcal{L}_j , outside and inside the nanostructures, connected by the continuity conditions across the interface of the j -th scatterer:

$$\mathcal{H}_j(t) = H^{(\text{out})}(\mathbf{r})|_{\mathbf{r} \rightarrow R_j^+(t)} = H^{(\text{in})}(\mathbf{r})|_{\mathbf{r} \rightarrow R_j^-(t)}, \quad (18a)$$

$$\mathcal{L}_j(t) = \left[\frac{\partial H^{(\text{out})}(\mathbf{r})}{\partial N_j} \right]_{\mathbf{r} \rightarrow R_j^+(t)} = \frac{\varepsilon}{\varepsilon_j^{(\text{in})}} \left[\frac{\partial H^{(\text{in})}(\mathbf{r})}{\partial N_j} \right]_{\mathbf{r} \rightarrow R_j^-(t)}, \quad (18b)$$

where the superscripts $+$ ($-$) indicate that the limit is

taken with \mathbf{r} from outside (inside) the scatterers. The incident (dipole) magnetic field on the surface in Eqs. (16) is given by

$$H^{(\text{dip})}(\mathbf{R}_l, \mathbf{r}_0) = \frac{\pi\omega^2((x_l - x_0)p_{0z} - (z_l - z_0)p_{0x})}{c^2 \sqrt{(x_l - x_0)^2 + (z_l - z_0)^2}} \times H_1^{(1)}\left(\frac{\omega}{c} \sqrt{(x_l - x_0)^2 + (z_l - z_0)^2}\right), \quad (19)$$

where $H_1^{(1)}$ is the first-order Hankel function of the first kind, and the dipole moment is defined as $\mathbf{p}_0 \equiv (p_{0x}, 0, p_{0y})$.

The resulting system of coupled integral equations is then solved numerically in order to determine the source functions (surface fields). Upon introducing these source functions into the initial Green's theorem integral equations, the electromagnetic field in the entire space can be obtained in a similar manner as in [30]. In particular, the electric field scattered back at the dipole position \mathbf{r}_0 , necessary to compute γ/γ_0 by means of Eq. (10), is determined through

$$E_x^{(p, \text{scat})}(\mathbf{r}_0) = -\frac{ic}{4\pi\omega\epsilon} \sum_j \int_{\Gamma} \left[\mathcal{H}(t) \frac{\partial^2 G^{(\text{out})}(\mathbf{r}_0, \mathbf{R}_j(t))}{\partial z \partial N_j} - \frac{\partial G^{(\text{out})}(\mathbf{r}_0, \mathbf{R}_j(t))}{\partial z} \mathcal{L}_j(t) \right] dt, \quad (20a)$$

$$E_y^{(p, \text{scat})}(\mathbf{r}_0) = 0, \quad (20b)$$

$$E_z^{(p, \text{scat})}(\mathbf{r}_0) = -\frac{ic}{4\pi\omega\epsilon} \int_{\Gamma} \left[\mathcal{H}_j(t) \frac{\partial^2 G^{(\text{out})}(\mathbf{r}_0, \mathbf{R}_j(t))}{\partial x \partial N_j} - \frac{\partial G^{(\text{out})}(\mathbf{r}_0, \mathbf{R}_j(t))}{\partial x} \mathcal{L}_j(t) \right] dt. \quad (20c)$$

With this formulation we also obtain the power emitted into the far field:

$$P_{\text{far}}(\omega) = \int_0^{2\pi} \frac{|S(\theta|\omega)|^2}{|E_0^i|^2} d\theta, \quad (21)$$

where the far-field scattering amplitude is

$$S(\theta|\omega) = i \left(\frac{c}{8\pi\omega\sqrt{\epsilon}} \right)^{1/2} \sum_j \int_{\Gamma_j} \left[i \frac{\omega}{c} \sqrt{\epsilon} [\eta_j'(t) \sin \theta - \xi_j'(t) \cos \theta] \mathcal{H}_j(t) - \mathcal{L}_j(t) \right] \times \exp \left[-i \frac{\omega}{c} \sqrt{\epsilon} [\xi_j(t) \sin \theta + \eta_j(t) \cos \theta] \right] dt. \quad (22)$$

Similar equations can be obtained for an *s*-polarized dipole source, but in this case working with the only non-zero component of the electric field [30].

C. Quantum Efficiency and Decay Rate Enhancements

We have seen that by treating the emitter as a semiclassical harmonic damped oscillator, we obtain the normalized decay rate (10). But it is necessary to determine the modification of the radiative and nonradiative decay rates separately, with varying quantum efficiency of the free dipole: for emitters with large intrinsic quantum efficiency, the interest lies on the modification of the radiative decay rate; by contrast, for emitters with low intrinsic efficiency, the enhancement of the apparent quantum efficiency is also relevant.

First of all, the total normalized decay rate γ/γ_0 is obtained through Eq. (10), where the electric field at the dipole position is numerically calculated from Eqs. (20). However, we need an independent calculation to extract the contributions from radiative and nonradiative decay rates separately. To that end, we consider the power emitted in the far-field (P_{far}) by a harmonic dipole oscillating at frequency ω , which is proportional to γ_r , the radiative decay rate [11]. This is numerically calculated from Eqs. (21) and (22). The power absorbed by the nanoantenna (P_{abs}) is proportional to the nonradiative decay rate γ_{nr} . Energy conservation requires that $P = P_{\text{far}} + P_{\text{abs}}$, where P is the total emitted power, so that [6,11]

$$\frac{P_{\text{far}}}{P} = \frac{\gamma_r}{\gamma_r + \gamma_{nr}}, \quad (23)$$

which accounts for the percentage of energy radiated into the far field from the total (radiated plus absorbed by the nanoantenna).

Finally, from the knowledge of γ/γ_0 and P_{far}/P , it is possible to obtain the variations of the quantum efficiency and the radiative and nonradiative decay rates, properly normalized, for an emitter with arbitrary intrinsic quantum efficiency η_0 , positioned near a nanostructure. The radiative decay rate γ_r , normalized by that of the free emitter γ_{r0} , is given by

$$\frac{\gamma_r}{\gamma_{r0}} = \frac{\mathcal{P}}{\eta_0} = \frac{\mathcal{P}}{\eta_0 + \alpha - 1}, \quad (24)$$

where we have defined $\alpha = \gamma/\gamma_0$ and $\mathcal{P} = P_{\text{far}}/P$. We use this convention also in the nonradiative case:

$$\frac{\gamma_{nr0} + \gamma_{nr}}{\gamma_{nr0}} = \alpha \frac{1 - \mathcal{P}}{1 - \eta_0} + \mathcal{P}. \quad (25)$$

The latter equation represents the power absorbed by the nanoantenna with respect to the intrinsic power lost by the free emitter. Obviously, Eqs. (24) and (25) are not defined in the case of $\eta_0 = 0$ or $\eta_0 = 1$, respectively, when the denominators are null. In such limiting cases, it suffices to multiply Eqs. (24) and (25) by η_0 and $1 - \eta_0$, respectively, obtaining in this manner a normalization with respect to γ_0 , in accordance with Eqs. (3) and (5).

In a similar manner, we calculate the apparent quantum yield:

$$\eta = \frac{\gamma_r}{\gamma} = \frac{\mathcal{P}}{\alpha} (\eta_0 + \alpha - 1). \quad (26)$$

When the intrinsic quantum yield is $\eta_0=1$, i.e., without intrinsic losses, we retrieve $\eta=\mathcal{P}$ that corresponds to the quantum efficiency for $\gamma_{nr0}=0$ [see Eq. (12)].

Commonly in fluorescence experiments, the excitation intensity is far below saturation. In this case, the (one-photon) fluorescence enhancement is determined through the expression [10,33]

$$\frac{I}{I_0} = \frac{\eta(\omega_{\text{fluo}})}{\eta_0} \left| \frac{\mathbf{p}_0 \cdot \mathbf{E}_{\text{loc}}(\mathbf{r}_0, \omega_{\text{abs}})}{\mathbf{p}_0 \cdot \mathbf{E}_{\text{exc}}(\mathbf{r}_0, \omega_{\text{abs}})} \right|^2, \quad (27)$$

where ω_{abs} and ω_{fluo} are the absorption and emission frequencies, respectively. The expression (27) shows that the key magnitude that governs the fluorescence enhancement is the product of the efficiency enhancement at ω_{fluo} and the pump enhancement at the excitation frequency ω_{abs} given by the enhancement of the local field intensity, which can be in turn calculated as in [30]. For that reason, one can expect an interesting phenomenology near to surface plasmon resonances (SPRs), where strong enhancements of the electromagnetic field and local density of states are possible at both frequencies.

3. RESULTS AND DISCUSSION

In this section, we study the modification of the fluorescence decay rates stemming from the strong perturbation of the local density of EM states near a silver nanoantenna. The nanoantenna consists of two silver rectangular nanowires (see inset Fig. 2) in vacuum ($\epsilon=1$). The dimensions of each rectangle are $20 \times 200 \text{ nm}^2$, with a gap of 10 nm. The dielectric function of silver [$\epsilon^{(\text{in})}(\omega) = \epsilon_{\text{Ag}}(\omega)$] is taken from [34]. Our aim is to explore the phenomenology associated with the modified emission in various configurations, unlike in [16] where only the specific experimental setup was considered in the calculations. Optimum configurations for different purposes can be thus designed.

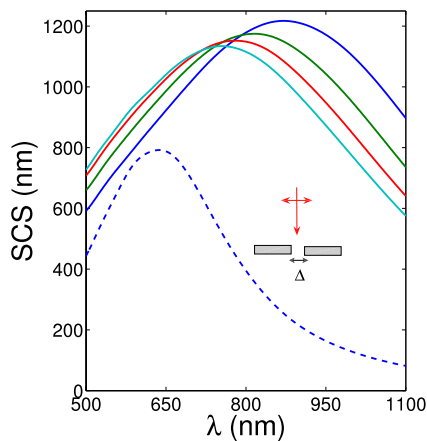


Fig. 2. (Color online) SCS for longitudinal polarization of silver dimer nanoantennas consisting of two rectangular nanowires of dimensions $20 \times 200 \text{ nm}^2$ with gap widths $\Delta=5, 10, 15, 20 \text{ nm}$ (solid curves, with redshifted bands as the gap decreases); a single rectangular nanowire (dashed curve).

A. Nanoantenna Optical Resonance

First of all, we examine the scattering properties of the nanoantenna. In Fig. 2 we show the scattering cross section (SCS) when the nanoantenna is illuminated with a plane wave impinging on the top with polarization along the dimer axis (i.e., with the electric field in the plane of the figure) for various gap widths Δ . Recall that the nanoantenna is bidimensional, thus extending in Fig. 1 and in the inset of Fig. 2 to $\pm\infty$ in the direction perpendicular to the plane of the figure. For the sake of comparison, we show in Fig. 2 the SCS of a single rectangle, too. Longitudinal dipolar SPRs are observed for all dimers, redshifted with respect to that of the single rectangle, due to the strong capacitive coupling [30,35,36]; in the limit of touching nanoantenna arms, the SCS of a single rectangle twice as long is retrieved, with the SPR wavelength close to twice that of the single rectangle [36]. In what follows, we focus on a dimer with gap width $\Delta=10 \text{ nm}$ (experimentally feasible), with the SPR wavelength at $\lambda \approx 814 \text{ nm}$, for which we expect a good coupling and outcoupling of a dipole emission positioned near the dimer, mediated by SPR excitation. Besides, at the frequency resonance a large enhancement of the electric field intensity is found at the gap center ($\sim 10^2$). The enhancement of the pump field with the relative enhancement of a dipole emission eventually positioned in the gap [see Eq. (27)] gives a particular interest to the study of emission properties about the resonance frequency for a dipole located in the vicinity of the gap.

B. Spectral Dependence

We first investigate in Figs. 3 and 4 the spectral dependence of the decay rates and quantum efficiencies, obtained from Eqs. (24)–(26), for an optical emitter, either vertically or horizontally polarized, located at the gap center of the dimer nanoantenna for two different gap widths that correspond to either uncoupled nanoantennas arms, $\Delta=100 \text{ nm}$ [see Figs. 3], or strongly coupled arms, $\Delta=10 \text{ nm}$ [see Fig. 4]. First of all, we observe in Fig. 4(b) that a strong enhancement ($> 10^2$) of the radiative decay rate takes place throughout the spectral region of the

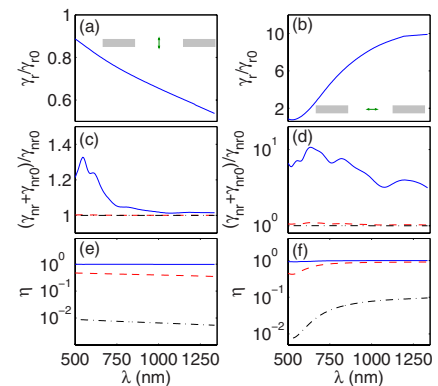


Fig. 3. (Color online) Spectral dependence of the normalized (a,b) radiative and (c,d) nonradiative decay rates, and (e,f) quantum yield, of a vertical emitter (left column) and of a horizontal emitter (right column). The emitter is placed at the center of the gap of the uncoupled nanoantenna with $\Delta=100 \text{ nm}$; each rectangular nanowire is $20 \times 200 \text{ nm}^2$. Intrinsic quantum yields: $\eta_0=99\%$ (solid curves), $\eta_0=50\%$ (dashed curves), and $\eta_0=1\%$ (dash-dotted curves).

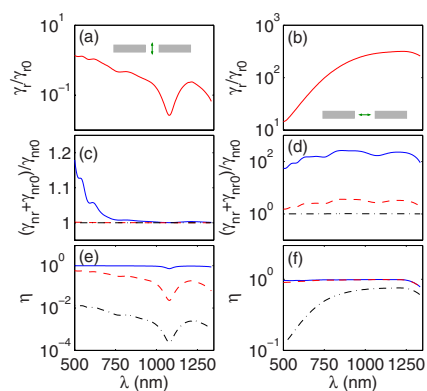


Fig. 4. (Color online) Spectral dependence of the normalized (a),(b) radiative decay rates; (c),(d) nonradiative decay rates; and (e),(f) quantum yield of a vertical emitter (left column) and of a horizontal emitter (right column). The emitter is placed at the center of the gap of the coupled nanoantenna with $\Delta=10$ nm; each rectangular nanowire is 20×200 nm². Intrinsic quantum yields are $\eta_0=99\%$ (solid curves), $\eta_0=50\%$ (dashed curves), and $\eta_0=1\%$ (dashed-dotted curves).

nanoantenna resonance in the case where the transition dipole is parallel to the dimer axis, its maximum being indeed redshifted with respect to that in the SCS. Recall that the intrinsic quantum efficiency has no impact on γ_r/γ_{r0} in Figs. 3(a), 3(b), 4(a), and 4(b), as expected. In contrast, the radiative decay rate for the transition dipole perpendicular to the dimer axis is not enhanced but reduced. This stems from the polarization dependence of the local density of the electromagnetic states at the gap center at the optical resonance, drastically enhanced (reduced) along (perpendicular to) the dimer axis. Note that the parallel/perpendicular radiative decay rates are weakly enhanced/reduced in the uncoupled case [see Figs. 3(a) and 3(b)].

The nonradiative decay rates, normalized as $(\gamma_{nr0} + \gamma_{nr})/(\gamma_{nr0})$ in Figs. 3(c), 3(d), 4(c), and 4(d), do depend on the intrinsic quantum efficiency, being larger the higher η_0 is. Qualitatively, the nonradiative decay rate for parallel polarization [see Fig. 4(d)] is also enhanced throughout the spectral range of the nanoantenna resonance (up to 10^2 for $\eta_0=99\%$); for perpendicular polarization [see Figs. 3(c) and 4(c)] it remains largely unaffected ($\gamma_{nr0} + \gamma_{nr})/\gamma_{nr0} \approx 1$ except for the region $\lambda < 600$ nm, where Ag bulk absorption is larger, as expected. In the uncoupled case [see Fig. 3(d)], again, resonant enhancements are substantially weaker.

The resulting quantum efficiencies are shown in Figs. 3(e), 3(f), 4(e), and 4(f) for intrinsic quantum efficiencies $\eta_0=1\%$, 50% , 99% . For high efficiency emitters with $\eta_0=99\%$, the margin for improvement is minimal; thus, the quantum efficiency remains largely unaffected throughout the spectral region of the figures for both the coupled and uncoupled nanoantenna. Only in the case of the vertical emitter, for which there is actually a strong inhibition of the radiative decay rate in the red-most part of Fig. 4(a) as commented above, is a significant reduction of the quantum efficiency also observed. This quantum efficiency decrease should be borne in mind when designing a nanoantenna for fluorescence enhancement. Note that a similar, even larger (nearly an order of magnitude) decrease is observed for vertical emitters with $\eta_0=50\%$ in

Fig. 4(e) as well as for $\eta_0=1\%$. Conversely, the enhancement of radiative decay rates has also a larger impact on quantum efficiencies when the intrinsic ones are smaller. Enhancements of the quantum efficiencies are shown in Fig. 4(f) for horizontal emitters with $\eta_0=1,50\%$ that are indeed qualitatively similar to those of the radiative decay rates in coupled nanoantenna [see Fig. 4(b)], provided that the nonradiative decay rates are more weakly enhanced to avoid quenching, as is the case [see Fig. 4(d)]. Quantitatively, enhancements of up to $\eta/\eta_0 \sim 10^2$ are found in the case of $\eta_0=1\%$. This might be crucial in designing nanoantennas for detecting low fluorescence molecules [37]. Finally, note that in the case of uncoupled dimer nanoantenna, Figs. 3(e) and 3(f), quantum efficiency enhancements are seen for $\eta_0=1,50\%$ that qualitatively follow the modification of the radiative decay rates in Figs. 3(a) and 3(b), though quantitatively weaker.

C. Spatial Dependence: 1-Nanoantenna

Let us now explore the dependence of the modification of decay rates as the horizontal emitter moves away from the gap center of the coupled nanoantenna at a fixed emission wavelength ($\lambda=814$ nm). First, the optical emitter is displaced vertically, i.e., perpendicular to the dimer axis; the corresponding decay rate enhancements and quantum efficiencies are shown in Fig. 5 (curves without symbols). The largest values of γ_r/γ_{r0} [see Fig. 5(a)] and $(\gamma_{nr0} + \gamma_{nr})/(\gamma_{nr0})$ [see Fig. 5(b)] are found at the gap center; both decrease as the distance is increased, reaching a minimum at a few tens of nanometers, from which the decay rates increase again leading to an oscillatory behavior as the distance exceeds ~ 100 nm. These oscillations have a period $\sim \lambda/2$, stemming from an interference effect due to the behavior of the nanoantenna as a weak reflecting film; such oscillations are well known from surface-enhanced fluorescence on metal surfaces and films [3]. For comparison, we also plot in Fig. 5 (curves with symbols) the dependence on vertical displacement, not from the gap center but from the center of one of the rectangles

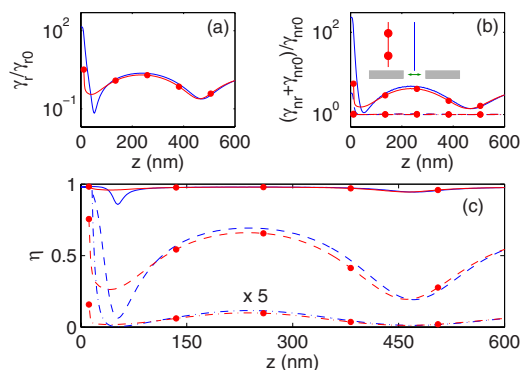


Fig. 5. (Color online) Normalized (a) radiative decay rates, (b) nonradiative decay rates, and (c) quantum yield of a horizontal emitter moving in the vicinity of the coupled nanoantenna vertically along two different paths: (i) from the center of the gap $z=0$ up to $z=600$ nm (curves without circles) and (ii) from 1.5 nm above the center of one of the rectangular nanowires up to $z=600$ nm (curves with circles). Intrinsic quantum yield of $\eta_0=99\%$ (solid curves), $\eta_0=50\%$ (dashed curves), and $\eta_0=1\%$ (dashed-dotted curves). $\Delta=10$ nm and $\lambda=814$ nm. Each rectangular nanowire is 20×200 nm².

of the dimer (starting at a distance of $z=1.5$ nm). The oscillations are indeed quite similar, although the enhancements of decay rates at closing distances on top of the nanowires are quantitatively smaller than those in the gap center.

Incidentally, note that the nonradiative decay rate enhancement remains moderate, even down to a distance $z \approx 1.5$ nm from the center of the rectangular nanowire; as a consequence, the onset of quenching takes place at a distance significantly smaller than that ($z \sim 10$ nm) for flat metal surfaces or thin films [3]. The physics underlying the decrease of quenching is the following: the spontaneous emission on surfaces/films is coupled to surface-plasmon polaritons, which are nonradiative modes that in turn contribute largely to γ_{nr} , unlike the coupling on nanoantennas to optical plasmon resonances, which are strongly radiative modes contributing mostly to γ_r .

With regard to quantum efficiencies [see Fig. 5(c)], the qualitative behavior follows that of decay rate enhancements, with larger quantitative impact on emitters with low η_0 .

D. Spatial Dependence: ||-Nanoantenna

Next, the horizontal optical emitter is fixed at a given height ($z=5, 10$ nm) and displaced horizontally from the gap center of the coupled nanoantenna dimer with $\Delta=10$ nm, scanning the upper side of one of the nanoantenna rectangular arms and away from it. The resulting decay rates and quantum efficiencies are shown in Fig. 6. The radiative decay rate in Fig. 6(a) exhibits a sharp peak at the gap center, followed by a sharp minimum on the rectangle corner facing the gap; γ_r then increases to a local maximum on top of the rectangle center and decreases when approaching the rectangle far end, where another local maximum occurs, approaching finally the limit $\gamma_r \rightarrow \gamma_{r0}$ upon moving away from the nanoantenna arm. The latter maximum in the decay rates at the dimer nanoantenna end is similar (though stronger) to that for monomer nanoantennas [38]. With regard to the nonradiative decay rates in Fig. 6(b), a qualitative behavior is expected similar to that of γ_r , with a strong quantitative dependence on η_0 .

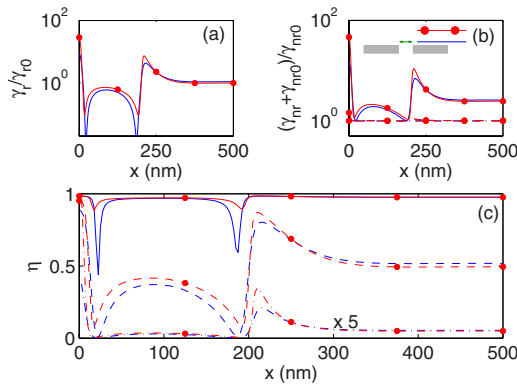


Fig. 6. (Color online) Normalized (a) radiative decay rates, (b) nonradiative decay rates, and (c) quantum yield of an horizontal emitter moving horizontally from above the gap center $x=0$ to $x=500$ nm to the right of the coupled nanoantenna at two fixed vertical positions: $z=5$ nm (curves with circles) and at $z=10$ nm (curves without circles). $\Delta=10$ nm and $\lambda=814$ nm. Each rectangular nanowire is 20×200 nm².

In turn, the quantum efficiencies, shown in Fig. 6(c), exhibit a strong dependence on γ_r and γ_{nr} : the qualitative behavior is similar to that of γ_r (provided that γ_{nr} is not predominant), but the quantitative values depend again on the intrinsic quantum efficiency. For large $\eta_0=99\%$, the minima of γ_r have a strong impact, leading to a reduction of η close to the rectangle ends. For small $\eta_0=1,50\%$, apart from such minima, strong enhancements of η are obtained at the gap center and close to the rectangle far end associated with a large value of γ_r/γ_{r0} .

E. Near and Far Fields

It is no doubt worth investigating the scattered field patterns associated to the dipole–nanoantenna system. We first show in Fig. 7 the intensity of the near field scattered by the dimer nanoantenna with $\Delta=10$ nm obtained from Eqs. (20). The horizontal dipole [see Fig. 7(a)] exhibits a strong coupling, with a near-field pattern distributed throughout the entire nanoantenna. This near-field pattern qualitative resembles that of the optical plasmon resonance [30,36], responsible in turn for the strong radiative outcoupling (as shown below). In contrast, the near-field pattern for the vertical dipole [see Fig. 7(b)] is strongly confined in the gap region, revealing a drastic inhibition of the dipole emission.

We now plot in Fig. 8 the far-field pattern resulting from both the isolated dipole emission and the scattering from the coupled nanoantenna with $\Delta=10$ nm; the latter scattered-field pattern has been calculated from Eqs. (22). The total far-field emission is shown for a horizontal and a vertical dipole located, respectively, at the dimer gap center (vertical lobes in Fig. 8) and at $z=5$ nm up from the gap center (large horizontal, down-shifted lobes in Fig. 8). Recall that isolated dipole emission in this geometry consists of two lobes [31], as explicitly shown for a vertical dipole in Fig. 8. It has been shown in [38] for monomer nanoantennas that the two-lobe dipole pattern corresponding to a fluorescent molecule can be altered by the presence of the nanostructure. The dipole–nanoantenna coupling is indeed stronger in our present dimer nanoantenna configuration.

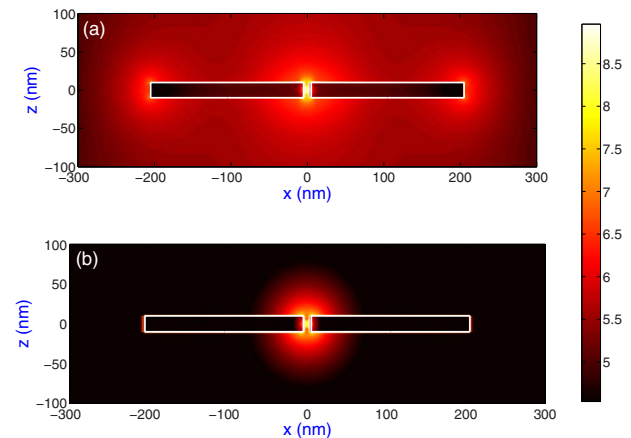


Fig. 7. (Color online) Near electric field intensity in logarithmic scale of (a) a horizontal dipole and (b) a vertical dipole placed at the gap center of a silver nanoantenna. Each nanowire has dimensions 20×200 nm² and the gap is $\Delta=10$ nm. The dipoles have a unitary dipole moment and emit at $\lambda=814$ nm. Only the field scattered by the nanoantenna is plotted.

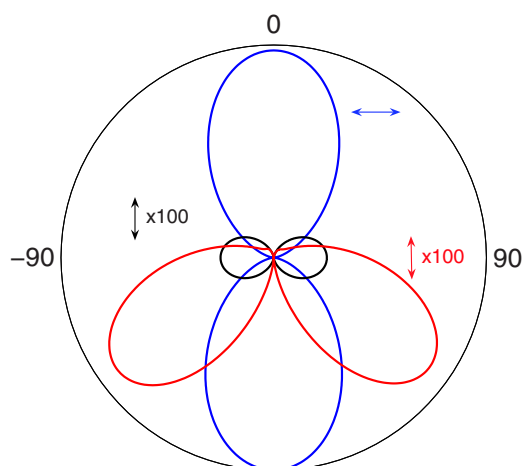


Fig. 8. (Color online) Far-field intensity patterns ($\lambda=814$ nm) of horizontal and vertical dipoles for a coupled dimer nanoantenna with $\Delta=10$ nm as in Fig. 7. The horizontal dipole is located at the gap center, whereas the vertical one is shifted $z=5$ nm up from the gap center. The contributions from both the direct dipole field and the field scattered by the nanoantenna are considered (see text). For comparison, the isolated dipole contribution ($\times 100$) is also shown for the vertical polarization (two small horizontally aligned lobes). Each rectangular nanowire is 20×200 nm².

In the case of the stronger coupling, namely, for the horizontal dipole, two vertical lobes perpendicular to the dimer axis are observed in Fig. 8. Qualitatively, the far field pattern of the nanoantenna (similar to a half-wavelength antenna) resembles that of the isolated vertical dipole, as reported in [36]. However, one has to bear in mind that the intensity scattered by the nanoantenna (as a result of the dipole–nanoantenna coupling) is at least two orders of magnitude larger than the intensity of the (isolated) dipole far field, revealing the nanostructure-enhanced spontaneous emission due to the strong modification of local density of electromagnetic states. In the case of the vertically polarized dipole, the dipole–nanoantenna coupling is weaker but leads to a qualitative behavior of the far-field pattern that merges both contributions, namely, the horizontal lobes of the isolated vertical dipole with the vertical lobes scattered by the nanoantenna as expected. This is revealed by the downward displacement of the resulting lobes with respect to the dimer axis in Fig. 8.

4. CONCLUSIONS

To summarize, we have presented a thorough theoretical study of the spontaneous emission of an optical emitter close to a metal nanostructure of arbitrary shape. A classical dipole model is used to express the radiative decay rate in terms of the electromagnetic field (strictly speaking, the electromagnetic density of states) scattered by the nanostructure, which we calculate on the basis of the rigorous formulation of the Green's theorem surface integral equations for a dipole source. In this regard, metal losses and the intrinsic nonradiative decay rate of the optical emitter are properly considered. Thus we present expressions for the radiative and nonradiative decay rates and quantum efficiency, valid in general for arbitrary intrinsic

quantum yield, that are directly related to magnitudes calculated numerically from the rigorous scattering formulation.

With this method, we investigate the modification of the radiative and nonradiative decay rates of a fluorescent molecule coupled to a resonant optical dimer nanoantenna. This is done for varying molecule position and dipole moment orientation. The largest enhancements occur at the dimer gap center for dipole moments parallel to the dimer axis; in addition, it should be mentioned that not only enhancements but also drastic reductions of decay rates are observed for perpendicular dipole moments at the gap center. In general, both radiative and nonradiative decay rates are strongly modified; however, the predominant enhancement of radiative decay rates over the nonradiative counterpart (responsible for quenching) result in an increase of the quantum efficiency, which can be as large as $\sim 10^2$ for emitters positioned in the gap. Finally, the strong coupling of the optical emitter to the nanoantenna is also studied in the resulting near- and far-field patterns, which exhibit significant qualitative and quantitative variations.

ACKNOWLEDGMENTS

J. A. Sanchez-Gil acknowledges support from the Spanish Ministerio de Ciencia e Innovación grant FIS2006-07894, the Consolider-Ingenio project Engineering METamaterials CSD2008-00066, and the Comunidad de Madrid through the MICROsistemas Ópticos SENsoRES network grant S-0505/TIC-0191. This work was also supported by the Netherland Foundation Fundamenteel Onderzoek der Materie (FOM) and the Nederlandse Organisatie voor Wetenschappelijk Onderzoek (NWO) and is part of an industrial partnership program between Philips and FOM.

REFERENCES

1. E. M. Purcell, "Spontaneous emission probabilities at radio frequencies," *Phys. Rev.* **69**, 681–681 (1946).
2. H. Kuhn, "Classical aspects of energy transfer in molecular system," *J. Chem. Phys.* **53**, 101–108 (1969).
3. R. R. Chance, A. Prock, and R. Silbey, "Molecular fluorescence and energy transfer near interfaces," *Adv. Chem. Phys.* **37**, 1–65 (1978).
4. M. S. Yeung and T. K. Gustafson, "Spontaneous emission near an absorbing dielectric surface," *Phys. Rev. A* **54**, 5227–5242 (1996).
5. W. L. Barnes, "Fluorescence near interfaces: the role of photonic mode density," *J. Mod. Opt.* **45**, 661–699 (1998).
6. L. Novotny, "Single molecule fluorescence in inhomogeneous environments," *Appl. Phys. Lett.* **69**, 3806–3808 (1996).
7. C. Hankel and V. Sandoghdar, "Single-molecule spectroscopy near structured dielectrics," *Opt. Commun.* **158**, 250–262 (1998).
8. K. T. Shimizu, W. K. Woo, B. R. Fisher, H. J. Eisler, and M. G. Bawendi, "Surface-enhanced emission from single semiconductor nanocrystals," *Phys. Rev. Lett.* **89**, 117401 (2002).
9. L. A. Blanco and F. J. García de Abajo, "Spontaneous light emission in complex nanostructures," *Phys. Rev. B* **69**, 205414 (2004).
10. M. Thomas, J.-J. Greffet, and R. Carminati, "Single-molecule spontaneous emission close to absorbing nanostructures," *Appl. Phys. Lett.* **85**, 3863–3865 (2004).
11. R. Carminati, J.-J. Greffet, C. Henkel, and J. M. Vigoureux,

- “Radiative and nonradiative decay of a single molecule close to a metallic nanoparticle,” *Opt. Commun.* **261**, 368–375 (2006).
12. H. Mertens, A. F. Koenderink, and A. Polman, “Plasmon-enhanced luminescence near noble-metal nanospheres: comparison of exact theory and an improved Gersten and Nitzan model,” *Phys. Rev. B* **76**, 115123 (2007).
 13. G. Baffou, C. Girard, E. Dujardin, G. Colas des Francs, and O. J. F. Martin, “Molecular quenching and relaxation in a plasmonic tunable system,” *Phys. Rev. B* **77**, 121101 (2008).
 14. P. Anger, P. Bharadwaj, and L. Novotny, “Enhancement and quenching of single molecule fluorescence,” *Phys. Rev. Lett.* **96**, 113002 (2006).
 15. S. Kühn, U. Hakanson, L. Rogobete, and V. Sandoghdar, “Enhancement of single-molecule fluorescence using a gold nanoparticle as an optical nanoantenna,” *Phys. Rev. Lett.* **97**, 017402 (2006).
 16. O. L. Muskens, V. Giannini, J. A. Sánchez-Gil, and J. Gómez Rivas, “Strong modifications of the spontaneous emission of light sources by single plasmonic nanoantennas,” *Nano Lett.* **7**, 2871–2875 (2007).
 17. W. L. Barnes, A. Dereux, and T. W. Ebbesen, “Surface plasmon subwavelength optics,” *Nature (London)* **424**, 824–830 (2003).
 18. E. Ozbay, “Plasmonics: merging photonics and electronics at nanoscale dimensions,” *Science* **311**, 189–193 (2006).
 19. H. Wang, D. W. Brandl, P. Nordlander, and N. J. Halas, “Plasmonic nanostructures: artificial molecules,” *Acc. Chem. Res.* **40**, 53–62 (2007).
 20. P. J. Schuck, D. P. Fromm, A. Sundaramurthy, G. S. Kino, and W. E. Moerner, “Improving the mismatch between light and nanoscale objects with gold bowtie nanoantennas,” *Phys. Rev. Lett.* **94**, 017402 (2005).
 21. P. Mühlischlegel, H.-J. Eisler, O. J. F. Martin, B. Hecht, and D. W. Pohl, “Resonant optical antennas,” *Science* **308**, 1607–1609 (2005).
 22. J.-J. Greffet, “Nanoantennas for light emission,” *Science* **308**, 1561–1563 (2005).
 23. T. H. Taminiau, R. J. Moerland, F. B. Segerink, L. Kuipers, and N. F. Van Hulst, “ $\lambda/4$ resonance of an optical monopole antenna probed by single molecule fluorescence,” *Nano Lett.* **7**, 28–33 (2007).
 24. L. Rogobete, F. Kaminski, M. Agio, and V. Sandoghdar, “Design of plasmonic nanoantennae for enhancing spontaneous emission,” *Opt. Lett.* **32**, 1623–1625 (2007).
 25. P. Bharadwaj and L. Novotny, “Spectral dependence of single molecule fluorescence enhancement,” *Opt. Express* **15**, 14266–14274 (2007).
 26. T. H. Taminiau, F. D. Stefani, and N. F. van Hulst, “Single emitters coupled to plasmonic nanoantennas: angular emission and collection efficiency,” *New J. Phys.* **10**, 105005 (2008).
 27. A. Mohammadi, V. Sandoghdar, and M. Agio, “Gold nanorods and nanospheroids for enhancing spontaneous emission,” *New J. Phys.* **10**, 105015 (2008).
 28. G. Sun, J. B. Khurgin, and R. A. Soref, “Plasmonic light-emission enhancement with isolated metal nanoparticles and their coupled arrays,” *J. Opt. Soc. Am. B* **25**, 1748–1755 (2008).
 29. N. A. Issa and R. Guckenberger, “Fluorescence near metal tips: the roles of energy transfer and surface plasmons polaritons,” *Opt. Express* **15**, 12131–12144 (2007).
 30. V. Giannini and J. A. Sánchez-Gil, “Calculations of light scattering from isolated and interacting metallic nanowires with arbitrary cross section by means of Green’s theorem surface integral equations in parametric form,” *J. Opt. Soc. Am. A* **24**, 2822–2830 (2007).
 31. J. D. Jackson, *Classical Electrodynamics* (Wiley, 1975).
 32. R. R. Chance, A. Prock, and R. Silbey, “Lifetime of an emitting molecule near a partially reflecting surface,” *J. Chem. Phys.* **60**, 2744–2748 (1974).
 33. V. Giannini and J. A. Sánchez-Gil, “Excitation and emission enhancement of single molecule fluorescence through multiple surface plasmon resonances on metal trimer nanoantennas,” *Opt. Lett.* **33**, 899–901 (2008).
 34. P. B. Johnson and R. W. Christy, “Optical constants of the noble metals,” *Phys. Rev. B* **6**, 4370–4379 (1972).
 35. J. Aizpurua, G. W. Bryant, L. J. Richter, F. J. García de Abajo, B. K. Kelley, and T. Mallouk, “Optical properties of coupled metallic nanorods for field-enhanced spectroscopy,” *Phys. Rev. B* **71**, 235420 (2005).
 36. O. L. Muskens, V. Giannini, J. A. Sánchez-Gil, and J. Gómez Rivas, “Optical scattering resonances of single and coupled dimer plasmonic nanoantennas,” *Opt. Express* **15**, 17736–17746 (2007).
 37. J. R. Lakowicz, “Radiative decay engineering 5: metal-enhanced fluorescence and plasmon emission,” *Anal. Biochem.* **337**, 171–194 (2005).
 38. T. H. Taminiau, F. D. Stefani, F. B. Segerink, and N. F. Van Hulst, “Optical antennas direct single-molecule emission,” *Nat. Photonics* **2**, 234–237 (2008).